Cell Surface Topography Is a Regulator of Molecular Interactions during Chemokine-Induced Neutrophil Spreading

Elena. B. Lomakina,[1] Graham Marsh,[1] and Richard E. Waugh[1,*]

[1]Department of Biomedical Engineering, University of Rochester, Rochester, New York

SUPPORTING MATERIALS

Description of lamellipodium diameter as a function of time.

Use of brightfield images to measure changes in the lamellipodial diameter with time required extrapolation backwards in time to determine the beginning of spreading. An alternative approach would have been to use fluorescence images to determine diameter. This works well when the cell label is bright and there is no significant lateral redistribution of receptors in the contact zone. Unfortunately this latter requirement is not met for L-selectin, and the CXCR-2 label was not nearly as bright as the other labels. We chose to use the brightfield images so that we could apply a consistent, reliable methodology for all of the different labels used. The best case for using fluorescence images to determined contact area was the non-specific Alexa label of the cell surface. In this case, there was close agreement between diameters measured in brightfield and those measured with fluorescence (although the fluorescent diameters tended to be smaller by approximately 0.5 μm). Based on these observations, the functional description of the change in diameter with time given in Eq. 6 was developed. As shown in Figure S1, the agreement between fitting the fluorescence data or the bright field data is very good.

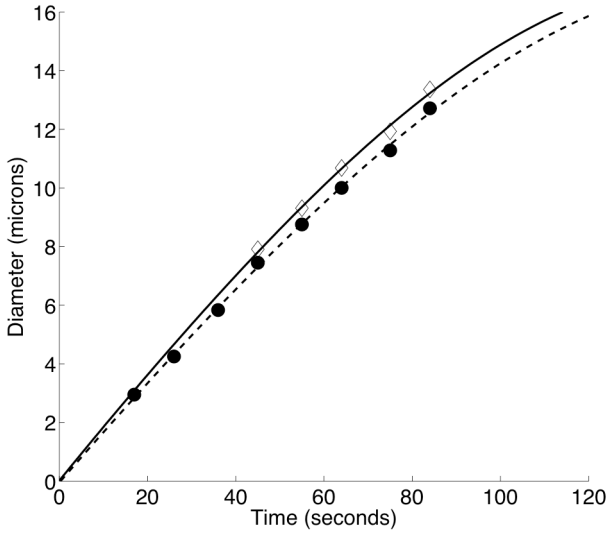

Figure S1. Lamellipodial diameter as a function of time. Filled circles represent measurements obtained from fluorescence images, and open symbols are from bright field images for the same cell. Fluorescence label was to CXCR-1. Although there is a small difference in the magnitudes of the diameters reflecting the limits of light resolution, both data sets show a logarithmic slowing of the rate of spreading over time. Solid and dashed curves are fits to Eq. 6. The fitted values for t_0 were used to adjust the two data sets to a common origin. The fitted values for the parameter A were 4.23 for the brightfield images and 4.51 for the epi-fluorescence images.

Modeling the surface topography deformation and fluorescence intensity

To evaluate the role that surface topography plays on the accessibility of adhesion molecules during leukocyte spreading, we developed a computational model of molecular distributions on realistic microvillus topography using our TIRF data to determine the distribution of molecules relative to the surface, and to estimate how the separation distance between molecules and the substrate change during cell spreading. The strength of the fluorescence signal obtained for a given microvillus is given by:

$$F = \iint_A P(x,y)E(z(x,y))\left|\frac{\partial z}{\partial x}\times\frac{\partial z}{\partial y}\right|\,\mathrm{d}x\mathrm{d}y \tag{S1}$$

where the absolute value term is the cross product, which resolves to: $\sqrt{1+\left(\frac{\partial z}{\partial x}\right)^2+\left(\frac{\partial z}{\partial y}\right)^2}$. The

coordinates x and y represent the projected coordinates on the substrate, z_s is the distance between the substrate and the cell membrane, E is the strength of the evanescent wave at a given distance z from the substrate, and P is the probability of finding fluorescent molecules at a given location above the surface. There are three basic components to the model:

1. Calculation of the strength of the evanescent wave $E(z)$as a function of distance from the glass surface;

2. Construction of a realistic description of the surface topography $z_s(x,y)$ and how it changes over time; and

3. Determination of the probabilistic distribution of individual receptors relative to the microvillus shape $P(x,y)$.

Evanescent Illumination

In TIRF experiments, the surface of the cell was illuminated with an evanescent wave at the coverslip surface. The penetration depth of the evanescent field depends on the angle of the incident beam on the coverslip interface, and therefore, it was important to characterize the intensity of the evanescent field as a function of distance from the coverslip under experimental conditions. According to basic theory, the intensity of an evanescent wave, E, at a depth z is given by the equation:

$$E(z) = E_0(\theta_i) \exp\left[\frac{-z}{\gamma(\theta_i)}\right] \tag{S2}$$

where E_0 is the evanescent constant and γ is the penetration depth of the wave, given by:

$$\gamma(\theta_i) = \frac{\lambda}{4\pi n_g \sqrt{\sin^2\theta_i - \sin^2\theta_c}} \tag{S3}$$

where θ_i is the angle of incidence at the interface, θ_c is the critical angle defined by the difference in reactive indices of the glass-sample interface, n_g is the index of refraction of the glass, and λ is the wavelength of the incident light. The incident angle of the laser, θ_i, is fixed so $\gamma(\theta_i)$ and $E_0(\theta_i)$ will be constant throughout the experiment.

Calibration of the evanescent wave

Mattheyses and Axelrod [2] showed that an evanescent field generated by a through objective TIRF system is best described by a superposition of two evanescent waves with different partial intensities and penetration depths. This superposition takes the form:

$$E(z) = \left(I_1 \exp\left[\frac{-z}{\gamma_1}\right] + I_2 \exp\left[\frac{-z}{\gamma_2}\right]\right) \tag{S4}$$

as a function of distance z away from the coverslip surface, where $I_{1,2}$ are the partial evanescent intensities and $\gamma_{1,2}$ are the evanescent penetration depths. To determine these coefficients, we used calibration beads labeled with an antibody conjugated to an AlexaFluor488 dye, with a surface intensity calibrated using flow cytometry. These beads were placed in the evanescent field and the fluorescence intensity was measured with one bead in the center of the field of view of the camera. The image was then analyzed with a custom Matlab script that subtracted the background noise, found the bead center and plotted the fluorescent intensity as a function of radius from the bead center. The bead diameter was known from the manufacturer specification

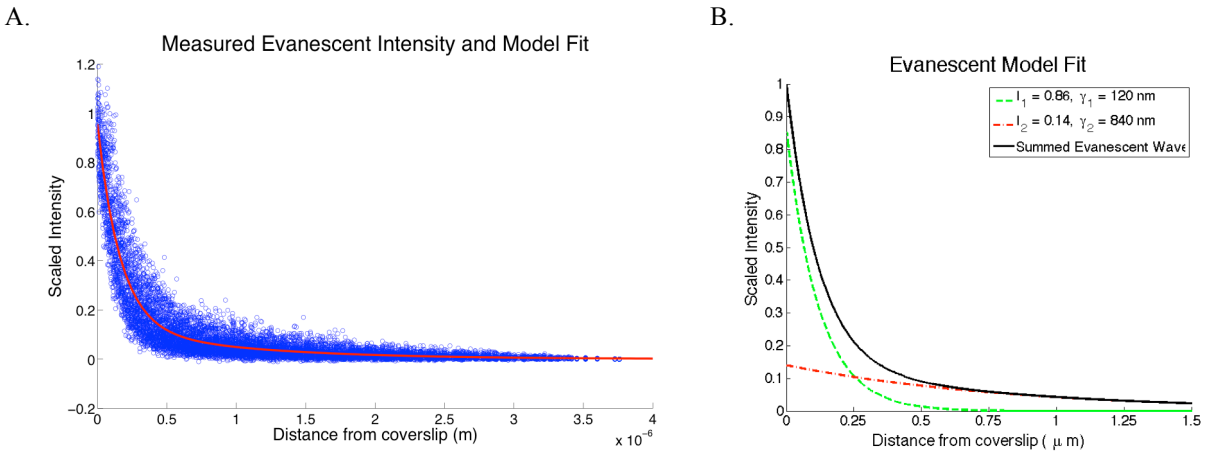

Figure S2. A. Example fit of double exponential to intensity measurements obtained from a calibration bead. Each point represents the gray scale value from an individual pixel in the image. Similar fits were conducted for 18 different beads. The resulting parameters are given in the text. B. Depiction of the two exponential curves that were summed to match the data. Parameter values are given in the inset.

and was confirmed with a brightfield image. With the bead diameter known, it was straightforward to convert intensity as a function of radius to intensity as function of distance from the coverslip surface. We then fit these data with Equation S3 to determine the evanescent parameters used in the experiment. Like Mattheyses and Axelrod, we found that a superposition of two evanescent waves accurately described our through-objective TIRF system. (See Figure S2.) The coefficients were determined to be $I_1 = 0.86 \pm 0.02$, $\gamma_1 = 0.12 \pm 0.02$ μm, $I_2 = 0.14 \pm 0.02$, and $\gamma_2 = 0.84 \pm 0.06$ μm, where ± values indicate the standard deviation for values calculated for data from each of 18 different beads. These values were consistent over multiple days of experiments.

Microvillus shape and distribution of heights

To model the cell surface topography we chose mathematical surfaces that most closely resembled the physical appearance of microvilli in electron micrographs. For simplicity, it was assumed that the microvilli shape was Gaussian-like, and, to emulate the ridge-like geometry, we took different characteristic lengths in x and y, such that the lengths (along the y-axis) of the microvilli were 10x longer than the width. We specified the height profile to be proportional to $\exp[-x^4]$, which we found gave the best visual match to microvilli seen in the electron micrographs. (We also tried microvilli models proportional to $\exp[-x^2]$, which appeared to be too pointed compared to the EM images, and $\exp[-x^6]$, which were too flat on top. (See Figure S3.)

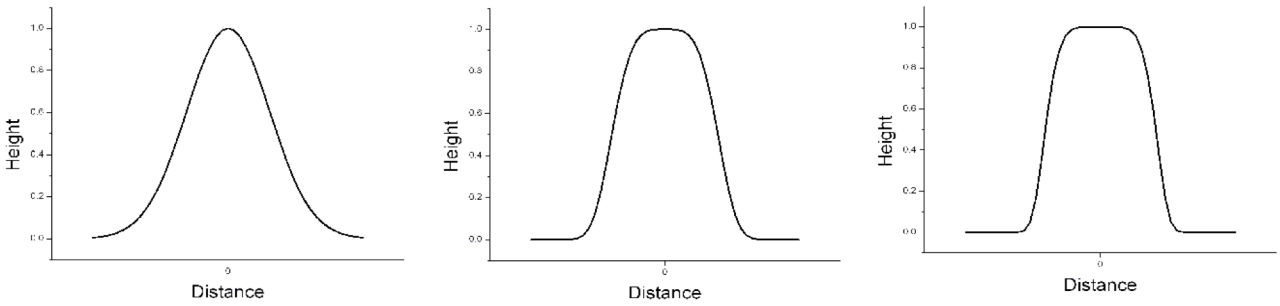

Figure S3. Visual comparison of alternative Gaussian-like profiles. Left panel: exp ($-x^2$), too pointed; Right panel: exp($-x^6$), too flat; Middle panel exp($-x^4$), about right. Compare to microvilli on the cell surface shown in Fig. 7 of the manuscript.

Thus, from the perspective of the cell surface, the height of the microvillus z_g was given as:

$$z_g(x,y) = h_i \exp\left[\frac{-x^4}{2\sigma_x^4} + \frac{-y^4}{2\sigma_y^4}\right] \tag{S5}$$

where h_i is the initial height of the microvillus (Fig. S4).

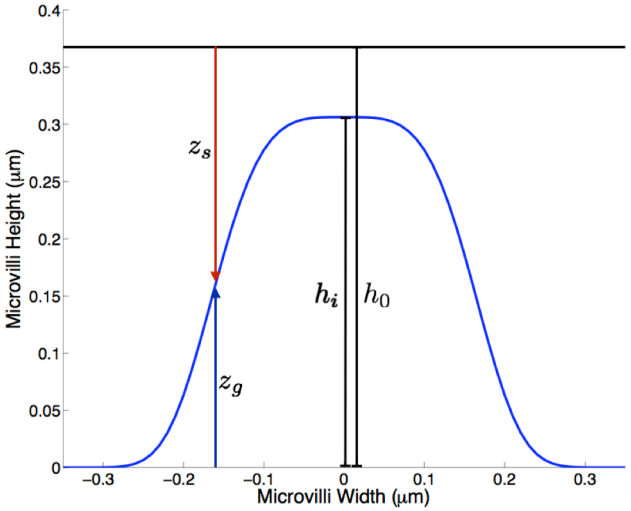

Figure S4. Coordinate scheme and definition of distances between the membrane, the substrate surface (at the top of the schematic) and the body of the cell.

Having settled on a generalized shape for the microvilli, we next sought to develop the proper distribution of microvilli heights. There were two experimental constraints on this distribution. The first was the magnitude of the change in TIRF signal between the resting state and the fully spread state for cells with a uniform surface label (Alexa-488) shown in Fig. 5A of the manuscript. If the microvilli heights are too large, the calculated difference in TIRF signal would be larger than what is measured, and if the heights are too small, the calculated change would be smaller than observed. The second constraint was the distribution of heights measured by Bruehl and colleagues [1] obtained from transmission electron micrographs of fixed and sectioned cells. The distribution of their measurements is well-fit by a lognormal distribution [3]. However, it is important to note that these are the heights measured from sectioning the cell surface, and may not reflect the distribution of vertical heights of individual microvilli. To generate a distribution of microvilli heights that were consistent with measurements of Bruehl et al., we first generated a set of Gaussian-like microvilli with different, discrete heights, with each height weighted by a proportion reflecting its relative prevalence on the surface. We then took 10,000 random slices through them and compared the distribution of apparent heights in the slices to the data of Bruehl. We allowed the slices to take any path through the *x*-*y* plane and allowed the slice to have a ± 45° angle from vertical in the z plane. We varied the heights of the microvilli in the series and the relative proportion of each microvilli height. For a maximum microvillus height h_0, we found a reasonable approximation of the log normal distribution was obtained when the microvilli heights were defined by the series: (1) = h_0/[1.0, 1.1, 1.2, 1.4, 1.6, 2.0, 2.4, 3.0] with probabilities $\{p_i\}$ = [0.02, 0.05, 0.09, 0.13, 0.16, 0.18, 0.18, 0.18]. Using this distribution and a value of h_0 = 550 nm, we obtain a good match to Bruehl's data (Fig. S5). While this distribution is likely not unique, it serves to mimic experimental observation.

Changes over time. In calculating the change in the surface topography over time, we assume that all microvilli impact the surface vertically and that microvilli begin to change shape only after they have contacted the surface. Thus, the tallest microvilli contact the glass surface and begin to spread first, and then smaller microvilli begin to spread when they come into contact with the surface as the longer microvilli heights decrease. The height is assumed to decrease on an exponential time course from its initial maximum as the cell spreads on the surface:

$$h_s(d) = h_0 \exp\left[\frac{-d}{\tau_s}\right] \tag{S6}$$

A.

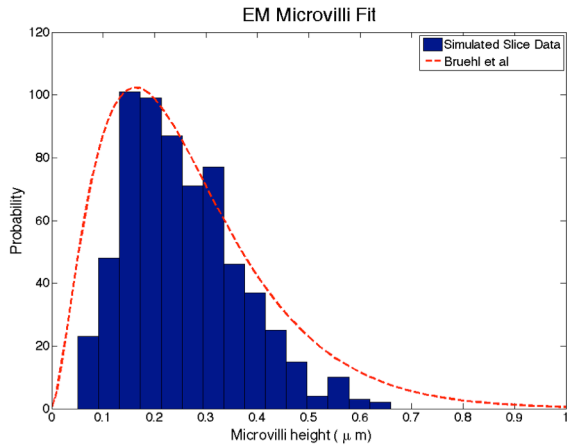

B.

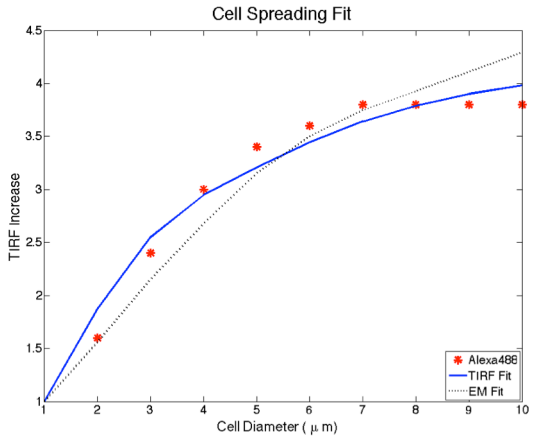

Figure S5. A. Histogram of modeled microvilli heights compared to the data of Bruehl et al. [1]. The dashed line is a log normal fit of the microvilli height histogram measured by Bruehl et al. in an EM study of microvillus lengths [1, 3]. The blue histogram is a selection of random slices through the series of model microvilli: h = h_0/[1.0, 1.1, 1.2, 1.4, 1.6, 2.0, 2.4, 3.0] with corresponding probabilities [0.02, 0.05, 0.09, 0.13, 0.16, 0.18, 0.18, 0.18]. The value for h_0 used to generate this matching histogram was 550 nm. The slices were allowed to take any path through the x – y plane, and were allowed to have a ±45◦ deviation from vertical in the z plane to simulate the act of randomly slicing fixed samples of leukocytes as part of the preparation for EM studies. **B.** Using the h_0 value or 550 nm needed to match Bruehl's data too large a difference in TIRF intensity is predicted (black dotted curve). A least squares fit to the TIRF data (red dots) gives a value of h_0 = 370 nm (blue curve). **C.** Slice data for the microvillus topography with h_0 = 370 nm. Dashed curve shows the fit to the Bruehl data for comparison.

C.

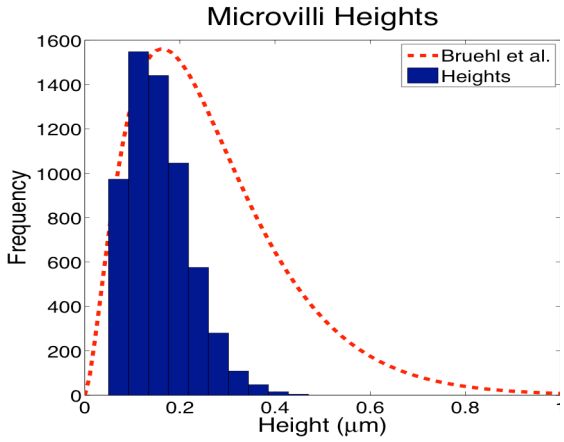

where h_s is the height of the spreading microvillus, h_0 is the characteristic height of the distribution (initial length of the longest microvilli), d is the diameter of the spreading lamellipodium (a surrogate for time), and τ_s is the spreading time constant, which has units of length because we are using the cell diameter as a measure of the progression of spreading. Note that this relationship results in all microvilli decreasing in height at the same rate once they have contacted the surface. Also note that the quantity h_s is the distance between the body of the cell and the substrate. For calculating the fluorescence signal that would be generated by a given microvillus, we need the distance from the substrate to a given point on the cell membrane z_s. The expression for this depends on whether the microvillus has started to spread or not. For spreading microvilli, $h_i = h_s$,

$$z_s(x,y) = h_s - h_s \exp\left[\frac{-x^4}{2\sigma_x^4} + \frac{-y^4}{2\sigma_y^4}\right] \tag{S7}$$

For microvilli that have not yet contacted the surface, $h_i < h_s$,

$$z_s(x,y) = h_s - h_i \exp\left[\frac{-x^4}{2\sigma_x^4} + \frac{-y^4}{2\sigma_y^4}\right] \tag{S8}$$

One last consideration is that the area of the cell membrane should not change as a result of the

microvillus collapse. To approximate this, we simply increase the area over which the TIRF signal is integrated in proportion to the decrease in the microvillus height (See Fig. S6). Thus the total TIRF fluorescence generated by a single microvillus is calculated by:

$$F_i = \int_{-y_i}^{y_i}\int_{-x_i}^{x_i} P(x,y)\sum_n I_n \exp\left[\frac{-\left(h_s - h_i \exp\left[\frac{-x^4}{2\sigma_x^4}+\frac{-y^4}{2\sigma_y^4}\right]\right)}{\gamma_n}\right] * \sqrt{1+h_i^2\left(\frac{x^6}{\sigma_x^8}+\frac{y^6}{\sigma_y^8}\right)\exp\left[\frac{-x^4}{\sigma_x^4}+\frac{-y^4}{\sigma_y^4}\right]}\,dx dy \quad \text{(S9)}$$

where x_i and y_i are set to maintain a the length of the cell membrane, $L_{x,y}$. The initial membrane length for each microvilli height in the series is calculated using the equation:

$$L_x = \int_{-x_i}^{x_i}\sqrt{1+\left(\frac{\partial z_g}{\partial x}\Big|_{y=0}\right)^2}\,dx$$
$$L_y = \int_{-y_i}^{y_i}\sqrt{1+\left(\frac{\partial z_g}{\partial y}\Big|_{x=0}\right)^2}\,dy \quad \text{(S10)}$$

and then new boundary values are calculated for each microvilli height such that the total membrane area is kept constant through the spreading process.

To obtain the total TIRF signal at a given instant in time, we simply sum over the different microvillus heights, with each contribution weighted by the corresponding probability of its occurrence:

$$F = \sum_i p_i F_i \quad \text{(S11)}$$

To predict the TIRF fluorescence as a function of time, we solved this equation by numerically integrating over the microvilli's area and found the total fluorescence for the cell at each spreading point and then summing over all values of the series *h*.

Determination of the coefficients h_0 and τ_s.

We labeled the entire cell surface with AlexaFluor488 to give the microvilli a uniform distribution of fluorescent labeling, and used these data to fit parameters h_0 and the spreading rate constant τ_s to be used throughout the simulation. A circular region with a 2.0 μm radius at the center of the cell contact region was selected as the region of interest, and the mean fluorescent intensity in TIRF was measured for this region at cell spreading diameters between 1 and 10 μm. (The diameter of contact was obtained from fits to the lamellipodim diameter measurements as described in manuscript.) The fold increase in fluorescence intensity was calculated by dividing the fluorescence

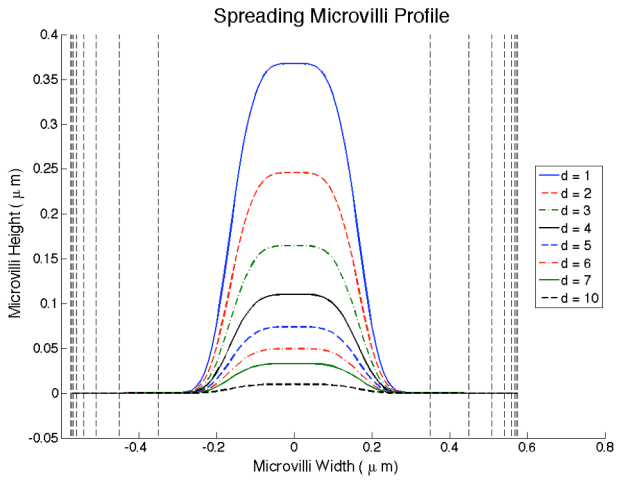

Figure S6. Height of the spreading microvilli at cell spreading diameters from 1 to 10 μm. The integration limits, $-x_i$ and x_i, used to maintain a constant cell membrane length for each microvilli height are shown as vertical dashed lines.

intensities by the initial fluorescence intensity when the diameter of the contact region was 1 μm. When these calculations were carried out for the distribution corresponding to that in Fig. S5A (with h_0 fixed at 550 nm) the predicted change in TIRF signal over the course of the spreading was greater than observed (black curve in Fig. S5B). In order to match the TIRF data, but still retain the lognormal distribution pattern obtained by Bruehl and colleagues, we performed a least squares regression, allowing both h_0 and spreading rate constant τ_s to vary. The results of the regression (Fig. S4B) gave h_0 = 368 nm with a 95% confidence interval: (319 nm, 416 nm), and growth constant τ_s = 2.49 μm with a 95% confidence interval: (1.63 μm, 3.36 μm). This height distribution (Fig. S5C) and spreading rate constant are the ones used in all subsequent calculations.

It is fair to note that the distribution we have used in the calculations is skewed toward smaller heights than those published by Bruehl and colleagues [1] (Fig. S5C), but these smaller heights were necessary in order to match our TIRF data. There are a few possible explanations for this. One consideration is that we assume that all microvilli are perfectly vertical as they approach the surface. In reality, it is likely that the longest microvilli will wind up at the edge of the contact zone as the cell settles into contact with the surface with the longest microvilli in the contact region likely forming a "tripod" supporting the cell. In this case the longest microvilli would contact the surface at an angle, resulting in a shorter distance between the fluorophores and the substrate. A second point is that the cells have already started to spread when we take the first TIRF data point, and so the longest microvilli should already have begun to decrease in height. A third potentially contributing factor is that we have restricted our slice angles to ± 45°, whereas some surface protrusions in the Bruehl study could have been sectioned at an even shallower angle, giving the impression of a greater villus height.

Thus from the measurements made on cells with a uniform surface label, we determine two parameters: The characteristic height h_0 of the microvillus height distribution, and the constant τ_s that characterizes the rate of height decrease with increasing diameter of the contact area.

Nonuniform distribution of fluorophores

As with the geometry of the microvilli, we experimented with different functions to describe the distribution of fluorescent molecules over the microvillus topography. We first tried a simple inverted Gaussian of the form:

$$P(x,y) = 1 - \exp\left[\frac{-x^2}{2\sigma_{fx}^2} + \frac{-y^2}{2\sigma_{fy}^2}\right] \tag{S8}$$

but found that we were unable to obtain a distribution of molecules with large enough differences between the microvilli tips and the valleys that when convolved with evanescent wave and the topography model was able to match the increases in TIRF signal we observed in the CXCR1 data. After some additional trials, we found that with a probability distribution proportional to $\exp[-x^6]$ we were able to approximate our experimental results. Initially, we used a procedure that allowed variation in the probability density in both the *x*- and *y*-directions, but discovered that the least square fits for σ_f in the *y*-direction either had little effect on the outcome, or produced non-physical results. Therefore we simplified our description, and only allowed variation in surface concentration in the x-direction, perpendicular to the long axis of the microvillus ridge:

$$P(x) = 1 - \exp\left[\frac{-x^6}{\sigma_f^6}\right] \tag{S9}$$

The width of the fluorescent distribution of molecules is thus characterized by the single constant σ_f . Fits of the data give values of σ_f for LFA-1 of 180 nm (170, 190), for CXCR1 of 220 nm (200, 230), and for CXCR2 of 170 nm (150, 190), where the numbers in parentheses indicate the 95% confidence intervals for the fitted parameters. These data indicate that LFA-1 is distributed away from the tip of the microvilli with a small percentage of molecules located on the shoulder of the microvilli, and the model puts nearly all of the molecules of CXCR1 the valleys away from the microvilli tip. (See Figure 5 in the manuscript.)

Beta Distribution

To test the sensitivity of our calculations to the functional form used to describe the nonuniform molecular distribution, we also fit the cell spreading data using a beta distribution to describe the variation in fluorophore concentration. In this case the probability of finding a fluorophore a distance *s* from the substrate was given by:

$$P(s;\alpha,\beta) = \frac{1}{B(\alpha,\beta)} s^{\alpha-1}(1-s)^{\beta-1} \tag{S10}$$

The parameters α and β can be fit to adjust the relative probability of finding molecules on the distribution, and the parameter B is a scaling factor such that the cumulative probability of the beta distribution is 1. Since the beta distribution only applies between the interval of [0, 1], we used d as a scaled height parameter such that $s(z) = z/h_s$ to shrink the beta distribution down to the microvilli height.

We used the beta distribution to fit the data in the same manner as the Exponential fits. We first used the spreading microvilli heights fit from the Alexa488 data and fit distributions of fluorescent molecules on top of those heights to find relative distributions. We then fixed the value of β = 1 and performed a least squares fit of the TIRF spreading to obtain the value of α for each fluorescent label. For LFA-1, α = 2.59 (2.23, 2.95); for CXCR-1, α = 3.94 (3.15, 4.73); and for CXCR-2, α = 2.39 (1.80, 2.97), where the numbers in parentheses give the 95% confidence intervals for the fitted values. Results are shown in Figure S8.

Increase in Molecular Accessibility

We use these model results to assess the percentage of molecules that are within 70 nm of the coverslip surface and would be accessible to form bonds with a substrate at the initial state, and compare this to the final state under the assumption that all molecules

A.

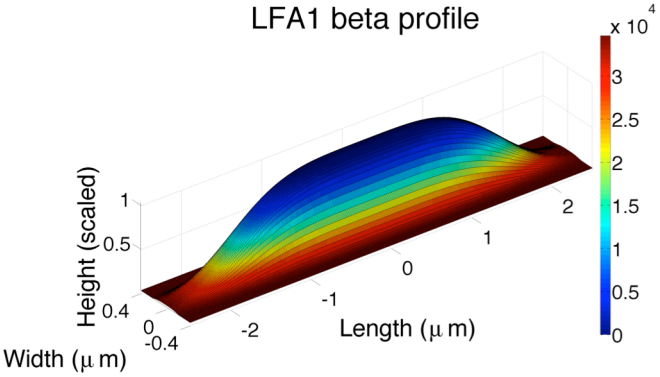

B.

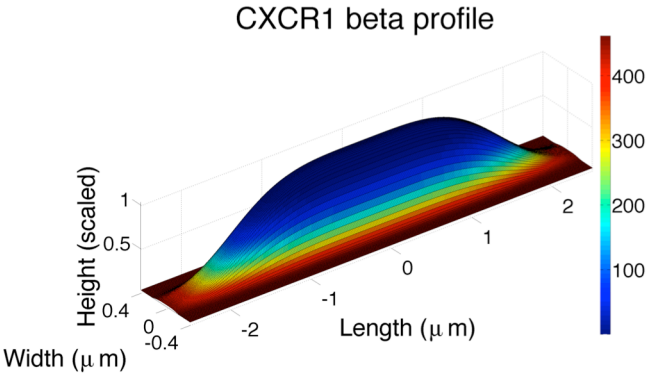

Figure S7. Distributions of LFA-1 (A) and CXCR1 (B) molecules from the model fit using the Beta-distribution. The *z*-axis is the scaled microvilli height $s = z/h_s$. The Beta distribution sequesters adhesion molecules to the valleys around the microvilli similar to the exponential model data with α as a free parameter. We found that the best fit of the LFA-1 data was α = 2.59, the best fit of the CXCR1 data was α = 3.94, and the best fit of the CXCR2 data was α = 2.39. Compare with the maps obtained using the inverted Gaussian distribution shown in Fig. 5 in the manuscript. Scale bars to the right map colors to molecular densities in #/μm².

are within 70 nm of the surface in a fully spread cell. Both the exponential model and the beta distribution model predict that there is a 1000-fold increase in accessible LFA-1 and CXCR2, and a 3000-fold increase in accessible CXCR1 once the cell has spread onto the glass substrate.

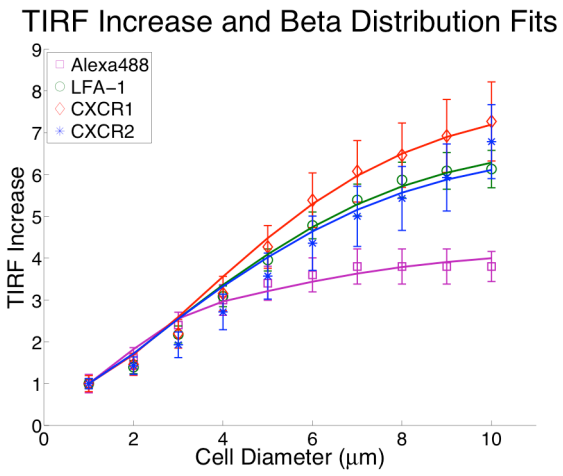

Figure S8. The fits to the spreading data using the beta distribution. The evanescent wave and the surface topography were determined as described above, and parameter α was varied for each fluorophore in a least squares regression to the data. (The parameter β was set to =1.0.) The distributions of molecules are shown in Figure S6. As was the case using the inverted Gaussian description, the beta distribution sequesters most of the LFA-1 and CXCR1 intensity in the valleys away from the microvilli tips.

Measurement error considerations.

Signal to noise

We estimated the signal to nose ratio (SNR) in our measurements by measuring the fluorescence signal over a 4.0 µm diameter region of interest at the center of the spreading cell, and dividing this by the standard deviation of sixteen same-sized regions of interest in the background. SNR varied from label to label depending on the brightness of the fluorescence signal, and for TIRF measurements, the SNR was a function of time, starting at a relatively low value, then increasing as the cell spread. Plots of the SNR as a function of spreading diameter are shown in Figure S9.

Label intensity variation

Variations in labeling intensity from cell to cell and from label to label were accounted for by normalizing measurements of fluorescence intensity in TIRF, either by the epifluorescence signal from the same cell, or a measurement of TIRF fluorescence early in the spreading process. We were not able to account for possible variability in the epifluorescence signal for different regions

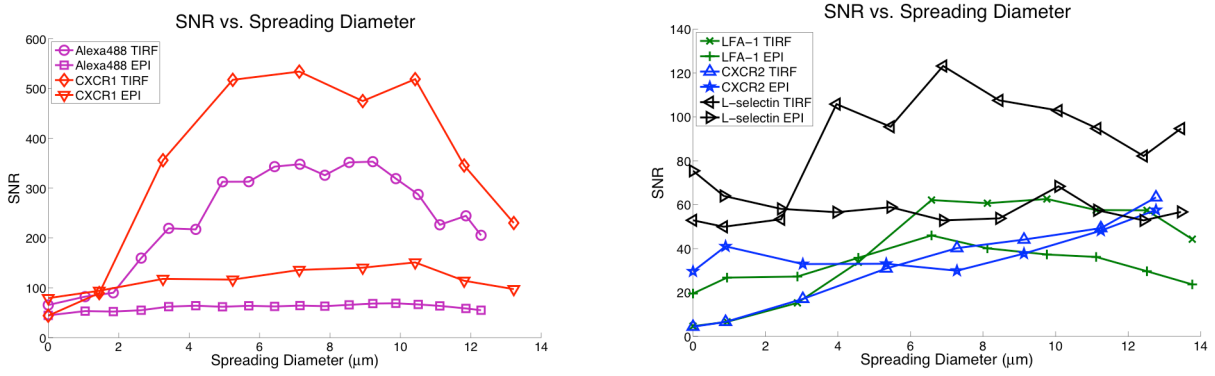

Figure S9. A. Signal to noise ratio (SNR) for the different labels used in the studies. A. Brighter labels (Alexa -488 and CXCR-1) showed SNR >50 for all measurements, both epi-illumination and TIRF. B. Dimmer labels (L-selectin, LFA-1, and CXCR-2) Showed SNR ratios in epi-fluorescence >20, and for TIRF measurements, SNR > 20 once the cell had spread to half of its maximum diameter. Each curve represents measurements obtained on a representative cell oeith the designated label. SNR was calculated using 4.0 µm diameter regions of interest, one at the center of the spreading region for the signal, and 16 measurements across the background of the image. The standard deviation of the 16 measured background means provided a measure of the noise in the image. SNR = Mean(signal)/SD(Bkgrnd).

of the cell surface. To assess how much variability there might be resulting from such variations, we captured an image of the cell in epifluorescence focused at the mid plane of the cell, and measured the mean fluorescence intensity over a series of approximately 145 segments 4.0 μm in length stepped around the cell perimeter. The standard deviation of those measurements was used to calculate a 95% confidence interval for the value obtained at a random location around the cell perimeter. For LFA-1 we concluded with 95% confidence that the mean intensity of a randomly chosen 4.0 μm segment was within ± 15% of the mean for the entire perimeter, and for CXCR-1, the segment intensity would be within ± 17% of the mean for the perimeter.

SUPPORTING REFERENCES

1. R.E. Bruehl, T.A. Springer, and D.F. Bainton. Quantitation of L-selectin distribu- tion on human leukocyte microvilli by immunogold labeling and electron microscopy. Journal of Histochemistry and Cytochemistry, 44(8):835–844, 1996.
2. A.L. Mattheyses and D. Axelrod. Direct measurement of the evanescent field profile produced by objective-based total internal reflection fluorescence. Journal of biomedical optics, 11:014006, 2006.
3. Hocdé, SA, O. Hyrien, and R. E. Waugh. Analysis of molecular accessibility in relation to cell surface topography and compression against a flat substrate Biophys. J. 97:369-378, 2009.

Movie Legends

Movie 1. Three views of a neutrophil with surface labeled non-specifically using Alexa Fluor 488 carboxylic acid –TFP spreading onto a glass slide coated with IL-8 – fractalkine stalk chimera. *Left*: brightfield, *Center*: epifluorescence, *Right*: TIRF. Move plays at approximately 30x actual speed.

Movie 2. Three views of a neutrophil with surface labeled with Alexa Fluor 488 conjugated anti-LFA-1 spreading onto a glass slide coated with IL-8 – fractalkine stalk chimera. *Left*: brightfield, *Center*: epifluorescence, *Right*: TIRF. Move plays at approximately 30x actual speed.

Movie 3. Three views of a neutrophil with surface labeled with Alexa Fluor 488 conjugated anti-CXCR-1 spreading onto a glass slide coated with IL-8 – fractalkine stalk chimera. *Left*: brightfield, *Center*: epifluorescence, *Right*: TIRF. Move plays at approximately 30x actual speed.

Movie 4. Three views of a neutrophil with surface labeled with Alexa Fluor 488 conjugated anti-CXCR-2 spreading onto a glass slide coated with IL-8 – fractalkine stalk chimera. *Left*: brightfield, *Center*: epifluorescence, *Right*: TIRF. Move plays at approximately 30x actual speed.

Movie 5. Three views of a neutrophil with surface labeled with Alexa Fluor 488 conjugated anti-L-selectin spreading onto a glass slide coated with IL-8 – fractalkine stalk chimera. *Left*: brightfield, *Center*: epifluorescence, *Right*: TIRF. Move plays at approximately 30x actual speed.

Movie 6. Brightfield (left) and fluorescence (right) images of a neutrophil labeled with Alexa 488 conjugated anti-LFA-1 spreading onto and engulfing a glass bead coated with IL-8 – fractalkine chimera. Movie plays at approximately 30x actual speed.

Movie 7. Brightfield (left) and fluorescence (right) images of a neutrophil labeled with Alexa 488 conjugated anti-CXCR-1 spreading onto and engulfing a glass bead coated with IL-8 – fractalkine chimera. Movie plays at approximately 30x actual speed.

Movie 8. Brightfield (left) and fluorescence (right) images of a neutrophil labeled with Alexa 488 conjugated anti-L-selectin spreading onto and engulfing a glass bead coated with IL-8 – fractalkine chimera. Movie plays at approximately 30x actual speed.

Note: The individual frames for each movie are shown in Fig. S10.

Figure 10

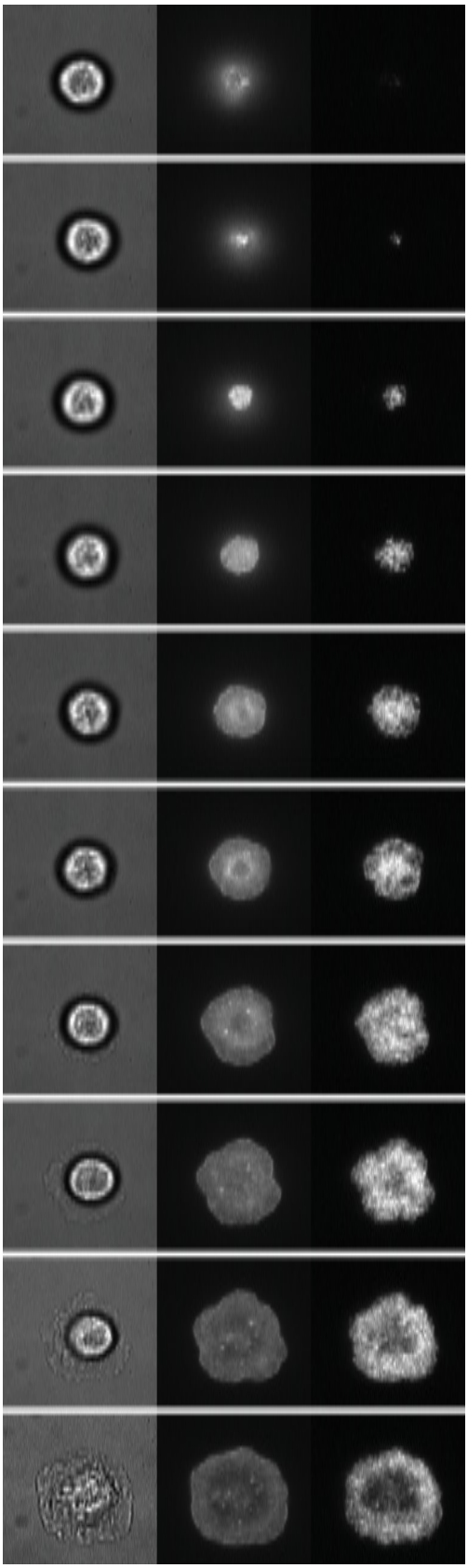

A. ALEXA

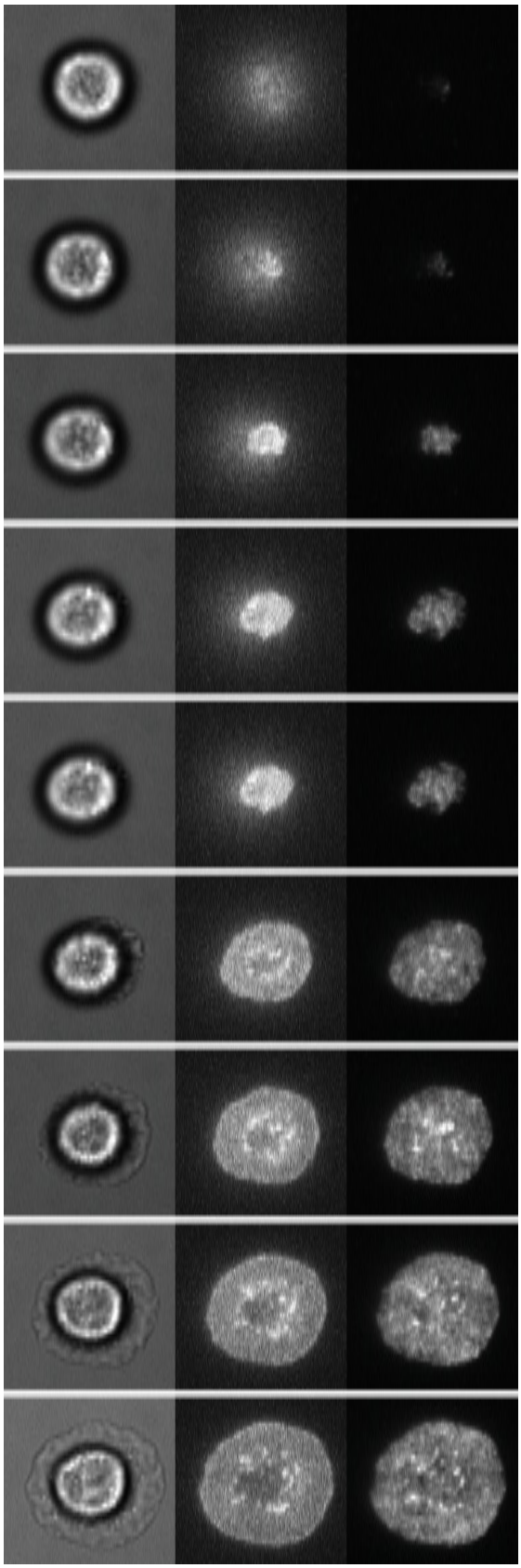

B. CXCR-1

Figure 9 (cont'd)

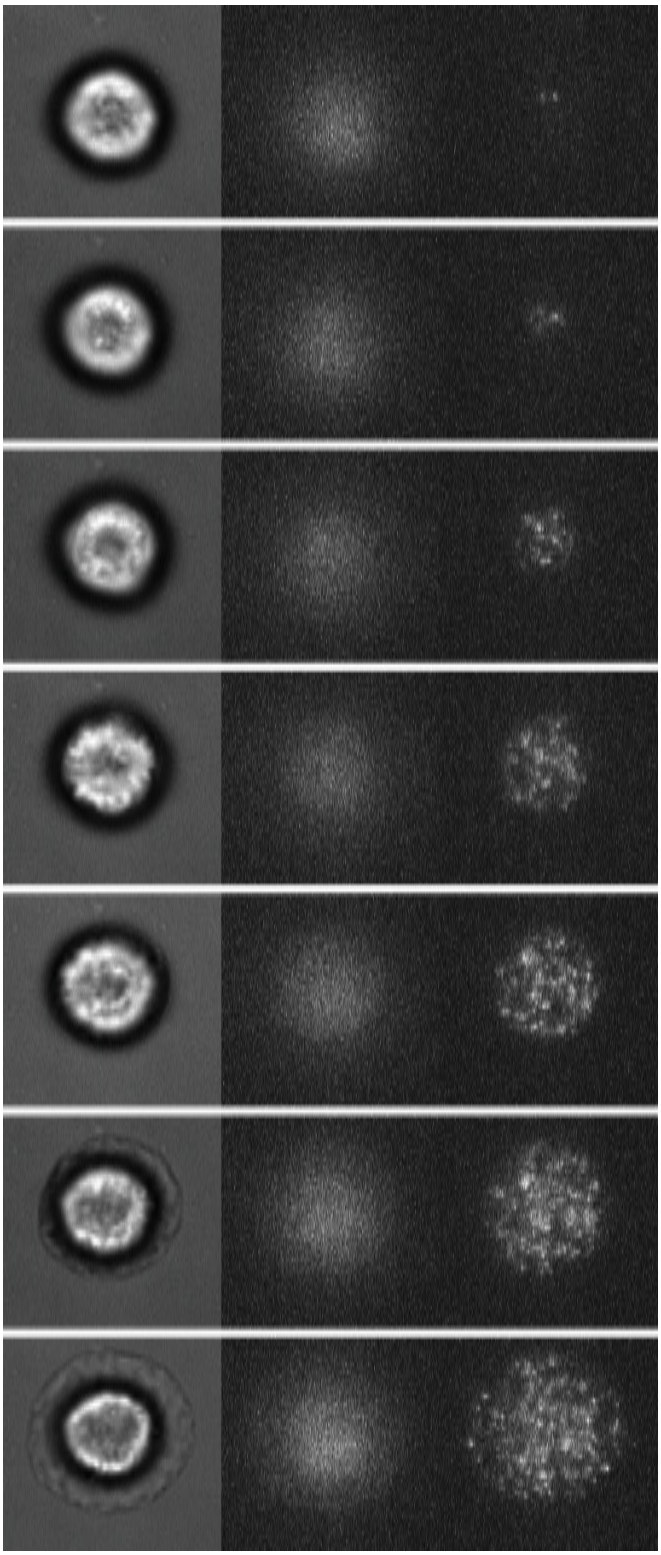

C. CXCR-2

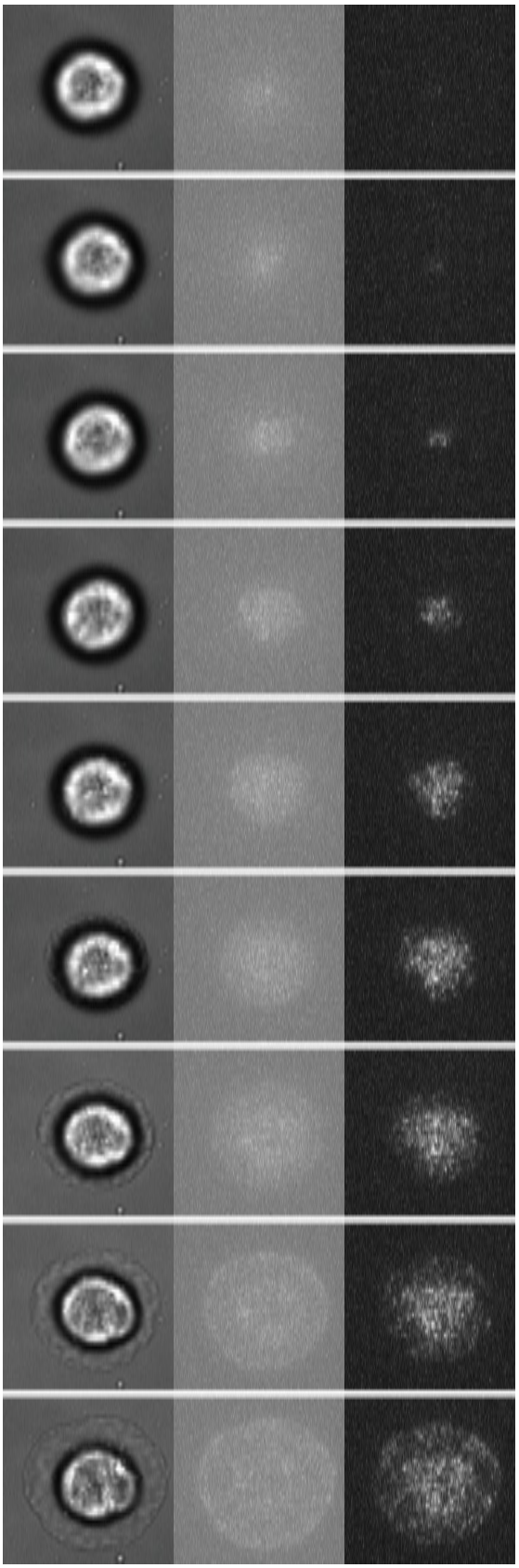

D. LFA-1

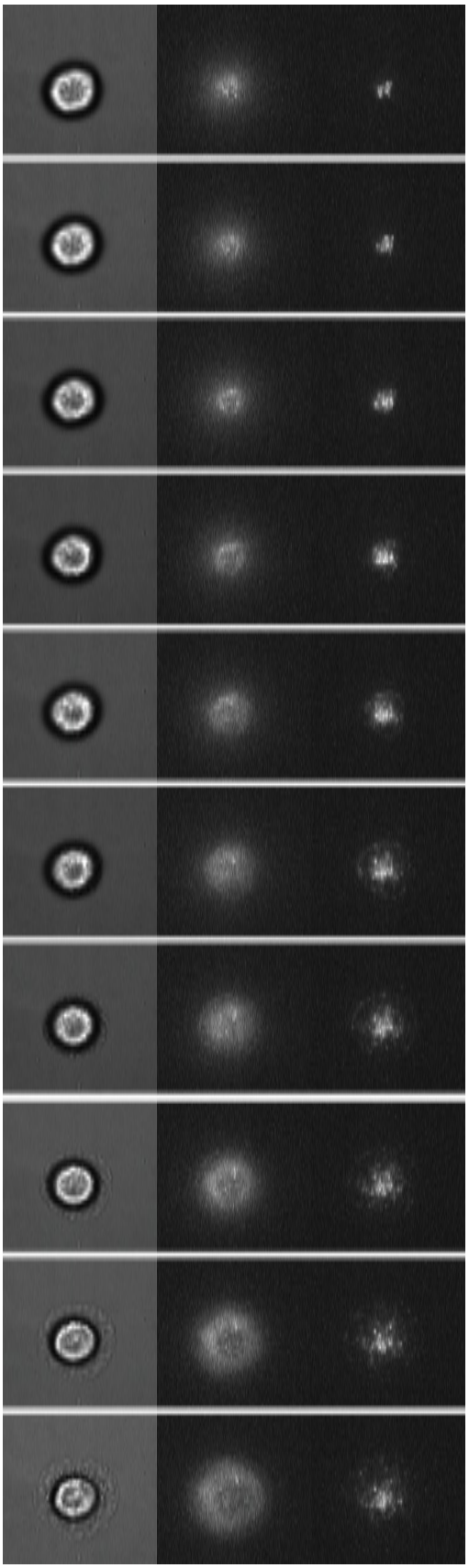

E. L-selectin

Figure S9. Individual frames from the movie sequences are shown here. The height of each individual frame is approximately 20 µm. A. Uniform ALEXA Label; B. CXCR-1; C. CXCR-2; D. LFA-1; E. L-selectin.